VERTICAL AND TEMPORAL VARIATION OF AEROSOL MASS CONCENTRATION AT MAGURELE – ROMANIA DURING EMEP/PEGASOS CAMPAIGN

M.M. CAZACU[1, 2], O. TUDOSE[1, 3], A. BOSCORNEA[4, 5], L. BUZDUGAN[6], A. TIMOFTE[1, 7], D. NICOLAE[8]

[1] *"Alexandru Ioan Cuza" University of Iasi, Faculty of Physics, Bulevardul Carol I, nr. 11, 700506 Iasi, Romania, Atmosphere Optics, Spectroscopy and Lasers Laboratory,*

[2] *Physics Department, Gheorghe Asachi Technical University of Iasi, 59A Mangeron Blvd., 700050 Iasi, Romania*

[3] *SC INOESY SRL, 21 Bradului Street, RO-700660, Iasi, Romania*

[4] *National Institute for Aerospace Research "Elie Carafoli" (INCAS), 220 I. Maniu Blvd, Bucharest, Romania, RO061126*

[5] *University of Bucharest, Faculty of Physics, P.O. BOX MG-11, Magurele, Romania, RO771525*

[6] *Romanian Air Traffic Services Administration (ROMATSA), 10 Ion Ionescu de la Brad Str., Bucharest, Romania, RO071952*

[7] *National Meteorological Administration, Regional Forecast Center Bacau, 3 Timpului Str., Bacau, Romania*

[8] *National Institute for R&D for Optoelectronics, 409 Atomistilor Str., Magurele, Ilfov, Romania, RO771525, E-mail: nnicol@inoe.inoe.ro*

Abstract. Natural (volcanic activity, desert dust storms) and anthropogenic (fuel combustion, biomass burning etc.) aerosols play an important role in climate changes, as they influence the solar radiation balance on Earth through light scattering and absorption processes. Additionally, both natural (e.g. Saharan dust) and anthropogenic (urban –traffic/industrial from big agglomerations aerosols) are acting as a trigger of the regional meteorology and weather forecast. This paper summarizes the temporal and vertical variation of mixed aerosol mass concentration near Bucharest, based on experimental data collected in the 2012 EMEP/PEGASOS campaign. From the series of experimental data collected we emphasize two cases, one for large biomass burning and one for a typical Saharan storm reaching the outskirts of Bucharest. The vertical mass concentrations profiles were determined based on the measurements performed with a multiwavelength depolarization Raman lidar. To assess the aerosol mass concentration using these lidar data, the authors are using the method proposed by Tesche et al., combined with forward simulations (i.e. OPAC). The results may contribute to describe, in an improved manner, the contribution of the mixed aerosols (low- or/and high-depolarizing particles) in the atmospheric simulations and models. It can also be used for operational purposes, such as near real time assessment of aerosol load (e.g. volcanic ash).

Key words: aerosol mass concentration, lidar, depolarization, EMEP/PEGASOS campaign

1. INTRODUCTION

Human activities influence the global climate that leads to major forcing on social and economic well-being. All these contributions to the earth's climate system are quantified by continuous monitoring of various atmospheric physical and chemical parameters (e.g. temperature, greenhouse gas and water vapor concentration or aerosol and cloud distributions). Due to their impact for climate and humans health, the quantification and dynamics of aerosols are of crucial importance. Aerosols are distributed inhomogeneously on both spatial and temporal scale. Their properties are highly influenced by the type of the source, but also by the meteorological conditions. Because of their variable microphysical and chemical properties, which are related to their composition and size, the characterization of aerosols on a global scale is very difficult [1]. Nevertheless, the accurate parameterization of aerosols is necessary in order to reduce uncertainties both in weather and climate models. In order to fulfill this requirement, in the last decades, some atmospheric transport and air quality models have been developed to integrate relevant information from ground or space-based instruments (lidar, radiometer, ceilometer, etc.). Although optical data are generally used for calibration or validation of satellite products, vertical profiles of the mass concentration are necessary in many applications, such as aviation safety, air quality, climatic modeling [2]. A substantial effort was paid in the last years to the retrieval of aerosol microphysical parameters from lidar measurements. The inversion of optical parameters is an ill-posed problem, and solutions cannot be uniquely obtained when a finite number of wavelengths are used.

Muller et al. developed an algorithm based on the concept of inversion with regularization to retrieve the aerosol microphysical parameters (effective radius, volume, surface-area, and number concentrations, and mean complex refractive index [3]. Regularization is performed by generalized cross-validation. Muller et al. made a sensitivity study based on this algorithm [4]. They used optical data derived from Mie-scattering calculations for monomodal and bimodal logarithmic-normal distributions in the particle size range between 0.01 and 10 μm, and a complex refractive index between 1.33 and 1.8 in the real part and between 0 and 0.1 in the imaginary part. These parameter ranges describe the properties of optically active atmospheric particles. They showed that two extinction channels are necessary in addition to the three elastic backscatter channels for determining the effective radius, surface-area, and volume concentrations to an accuracy of ±50%, the real part of the complex refractive index to ±0.1, and the imaginary part to ±50%.

The Lidar/Radiometer Inversion Code (LIRIC), which combines the multiwavelength lidar with sun photometry data sets, allows retrieving vertical profiles of particle optical and microphysical properties, separately for fine-mode and coarse-mode particles. LIRIC uses three elastic backscatter channels and photometer-derived volume-specific backscatter and extinction coefficients.

Applying the LIRIC method to evaluate its potential to retrieve optical and microphysical properties of non-spherical aerosols, Wagner demonstrated very good results for volume and mass concentration profiles of unregulated shaped particles [5]. Forward simulation of optical properties takes into account various aerosol types, for which a certain composition is assumed. In principle, such models could be used to provide look-up tables for the inversion of optical information. A more complex situation is when atmospheric layers contain a mixture of different aerosol types, with different scattering and absorption properties. In these cases, the probability to find the proper aerosol class by using simulated data is sufficiently low. Moreover, calculation of the mass concentration becomes impossible without a preliminary knowledge of the aerosol chemical composition [6].

In this paper, the variation of aerosol mass concentration observed during EMEP/PEGASOS campaign at Magurele (located 6 km from Bucharest), Romania is presented. EMEP/PEGASOS campaign, an intensive European measurement campaign focusing on aerosols (EMEP) and oxidizing capacity (PEGASOS), started at June 8th, 2012 and ended at July 17th, 2012. Based on the lidar measurements performed at Magurele EARLINET station (lat. 44.35N, long. 26.03 E, 93 m ASL) each day around sunset, we analysed the vertical and temporal variations of aerosol mass concentration for the entire period. The instrument used is a multiwavelength depolarization Raman lidar, operating at 1064, 532 and 355 nm and collecting at 1064, 532 cross, 532 parallel, 355, 607, 387 and 408 nm. Using combined elastic and Raman detection, the backscatter and the extinction coefficients were retrieved independently [7], and lidar ratio at 355 and 532 nm was computed with practically no assumption. To assess the aerosol mass concentration using these lidar data, the authors are using the method proposed by Tesche et al., combined with forward simulations (i.e. OPAC) [8]. In their research, Tesche et al. separate the contribution of fine and coarse particles to the total optical parameter (the backscatter coefficient), assuming that fine particles are generally spherical, and therefore not depolarizing, while coarse particles are completely non-spherical, and therefore strongly depolarizing. This assumption can be applied for continental sites, where maritime aerosols are not present. Maritime aerosols contain also spherical coarse particles, which cannot be discerned from the fine particles based on depolarization separation [9].

In our study, the separated backscatter profiles are further used to compute the separated extinction profiles, by using the measured lidar ratio and the assumed mean lidar ratio of each mode. Forward simulated optical data provided by the Optical Properties of Aerosol and Clouds software package and assumption of a particular type of particles for fine and respectively coarse modes allow us to compute the separated and total mass concentration of mixed aerosols [10]. The results reported in this paper may contribute to describe, in an improved manner, the contribution of the mixed aerosols (low- or/and high-depolarizing particles) in the atmospheric simulations and models. It can also be used for operational purposes, such as near real time assessment of aerosol load (e.g. volcanic ash).

2. INSTRUMENTATION AND METHODS

The lidar

For this study, we used backscatter and extinction coefficients profiles obtained using a multi-wavelength Raman lidar (RALI) of the National Institute for Research and Development in Optoelectronics (INOE), Magurele – Romania, part of EARLINET (European Aerosol Research Lidar Network) [11]. Since June 2008, RALI is operating in daytime configuration (elastic channels only) and nighttime configuration (elastic and Raman channels) following EARLINET schedule [12]. Most of the detection channels have both analog and photon counting acquisition, which allow a good signal-to-noise ratio up to 15 km altitude, depending on the atmospheric conditions [13]. A polarizing beamsplitter cube is used to measure the atmospheric backscatter signals in two receiving channels, parallel - and cross-polarized with respect to the plane of the liniar polarized of the laser beam. This leads to the measurement of the depolarization introduced by the scatterers to the linearly polarized laser beam. Depolarization is directly related to the shape of the particles, allowing to distinguish between spherical (water clouds, biomass burning smoke) and non-spherical particles (mineral dust, ice clouds) [14].

A more quantitative characterization of aerosol's shape is provided by the linear volume depolarization ratio δ^V, which is defined as the ratio of the cross–polarized lidar return signal to the parallel-polarized backscatter signal [15]:

$$\delta^V(Z) = \frac{\beta_{\perp}^{total}(Z)}{\beta_{\parallel}^{total}(Z)} = \frac{P_{\perp}(Z)}{P_{\parallel}(Z)} \tag{1}$$

For an ideal system, this would be equal to the ratio of the received signals in cross and parallel channels. For a non-ideal system, a calibration function taking into account the whole system depolarization effects and the differential detection on the two channels has to be considered [15].

Calculation of the mass concentration requires quantitative measurement of the particle depolarization [8]:

$$\delta^{part} = \frac{\beta_{\perp}^{part}}{\beta_{\parallel}^{part}} = \frac{\left(1+\delta^{mol}\right)\cdot\delta^V\cdot R - \left(1+\delta^V\right)\cdot\delta^{mol}}{\left(1+\delta^{mol}\right)\cdot R - \left(1+\delta^V\right)} \tag{2}$$

where R is the backscatter ratio:

$$R = \frac{\beta^{mol} + \beta^{part}}{\beta^{mol}} \tag{3}$$

and δ^{mol} is the system-dependent molecular depolarization, which can be estimated for the aerosol-free regions considering the measured system function. In order to derive the mass concentration for low and high-depolarizing components of aerosols, it is therefore necessary to estimate accurately the calibration function.

The lidar system used in this study makes use of the ±45^{o} calibration method developed by Freudenthaler et al. [15].

The model

The OPAC (Optical Properties of Aerosols and Clouds) software package provides microphysical and optical properties of some general typical cases of atmospheric components (six water clouds, three ice clouds and ten aerosol components) [10]. Based on the microphysical data (size distribution and spectral refractive index), depending on the geometry of the particles (spherical for aerosols and cloud droplets and hexagonal columns for cirrus clouds), mass-extinction ratio, asymmetry parameter and lidar ratio for various aerosol types are computed. Aerosols in OPAC are described by an internal mixture of various components (insoluble, water soluble, soot, sea salt, mineral and sulfate droplets), in various proportions. Custom types of aerosols can be set by the user by changing the components and their proportions. Additionally, all optical properties can be computed for 8 classes of relative humidity, which is important especially for hygroscopic particles like smoke. Simulations in OPAC give us a good estimation of the mass-extinction efficiency, a conversion parameter that can be used to calculate mass concentration from measured extinction, assuming a certain aerosol type.

The approach described by Tesche et al. and particle linear depolarization ratio allows separating the spherical and non-spherical aerosols contributions to the optical properties [16]. This method was developed during two measuring campaigns (SAMUM-1 for pure dust in Morocco and SAMUM-2 for linear particle depolarization ratio retrieval). According to their method, the total aerosol backscatter coefficient can be decomposed in the contribution from dust and contribution from smoke, using the measured particle linear depolarization ratio:

$$\beta_{dust}^{part} = \beta_{total}^{part} \cdot \frac{\left(\delta_{total}^{part} - \delta_{smoke}^{part}\right) \cdot \left(1 + \delta_{dust}^{part}\right)}{\left(\delta_{dust}^{part} - \delta_{smoke}^{part}\right) \cdot \left(1 + \delta_{total}^{part}\right)} \tag{4}$$

where δ_{total}^{part} is the measured particle linear depolarization, β_{total}^{part} is the measured aerosol backscatter coefficient, and δ_{dust}^{part} and δ_{smoke}^{part} are the assumed mean values for the linear particle depolarization of the two pure aerosol components (dust and smoke).

We applied this method to the three days continuous measurements dataset acquired during the EMEP/PEGASOS campaign at Magurele - Romania, in order to assess the vertical mass concentration of high-depolarizing particles (mineral dust) and low-depolarizing particles (smoke / biomass burning aerosol) and their temporal variation [17]. Models and satellite imagery were then used to estimate the source and type of the detected aerosol layers. Three complementary data sources were used in this paper: DREAM (The Dust Regional Atmospheric Model) (http://www.bsc.es/projects/earthscience/DREAM/) forecast model developed by Nickovic et al. which is an integrated modelling system describing the dust cycle in the atmosphere [18], HYSPLIT (Hybrid Single Particle Lagrangian Integrated

Trajectory model) (http://www.arl.noaa.gov/ready/hysp_info.html), which is the newest version of a complete system for computing simple air parcel trajectories, and MODIS (Moderate Resolution Imaging Spectroradiometer), which provides hotspots of fire and burned area information to natural resource managers around the world [19].

RESULTS AND DISCUSSIONS

Atmospheric aerosols from both anthropogenic (e.g. sulfate, biomass burning smoke, black carbon) and natural sources (e.g. mineral dust and sea salt) introduce large temporal and regional variations in the heat balance of the Earth by scattering and absorbing solar radiation, absorbing and emitting terrestrial infrared radiation, and influencing their ability to nucleate cloud droplets [20].

During the EMEP/PEGASOS campaign (June 8th, 2012 – July 17th, 2012), a large spectrum of aerosol types was detected. In this section we present two representative cases, a smoke case from July 11th, 2012, and a Saharan dust case from July 15th, 2012.

For these two cases, using the theory and methods described, we calculated the temporal and vertical variation of mixed aerosol mass concentration at Magurele station.

Case 1. Smoke on July 11th, 2012 at Magurele

Biomass burning is the burning of living and dead vegetation. It includes the human-initiated burning of vegetation for land clearing and land-use change as well as natural, lightning-induced fires. Scientists estimate that humans are responsible for about 90% of biomass burning with only a small percentage of natural fires contributing to the total amount of vegetation burned.

Burning vegetation releases large amounts of particulates (solid carbon combustion particles) and gases, including greenhouse gases. Between July 11th 2012 23:33:02 UTC and July 12th 2012, 00:03:02 UTC, a well-defined smoke layer at 2500 m was detected by the lidar above Magurele, Fig. 1a. This layer is visible both in the 1064nm, Fig. 1a: top of the layers are marked in black), and 532 nm range corrected signal, Fig. 1b.

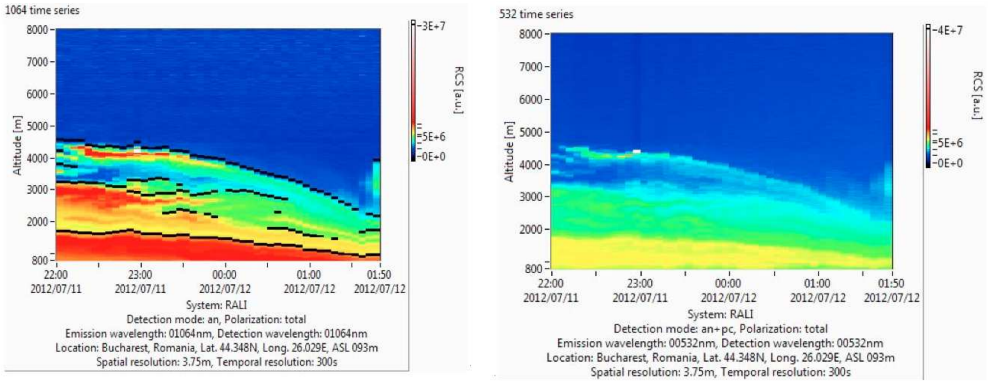

(a) (b)

Fig. 1 - Vertical and temporal distribution of aerosol layers on July 11th, 2012: a) 1064 nm range corrected signal and b) 532 nm range corrected signal measured by the lidar.

Applying the theory used by Tesche et al. the backscatter and extinction coefficient vertical profiles for depolarizing and non-depolarizing particles are obtained, Fig. 2a, Fig. 2b [8]. We used a mean characteristic value of 30% linear particle depolarization ratio for dust, and a value of 3% for smoke, respectively.

The mean characteristic lidar ratio was considered 30 sr for dust and 80 sr for smoke. Note that the vertical atmospheric column is characterized by a mix of depolarizing (dust) and non-depolarizing (smoke) particles, which contributes differently to the backscatter and extinction coefficient. Although the separated backscatter profile seems similar up to 5 km, the corresponding extinctions are significantly different.

This is due to the absorption properties of smoke particles, much larger than of the dust. Fig. 2c shows the retrieved mass concentration profiles for dust (black line), smoke (red line) and total aerosols (green line).

The profiles were obtained from separated extinction profiles in Fig. 2b multiplied by the considered 1064 nm mass-extinction efficiencies for dust (0.4 m^2/g) and smoke (0.5 m^2/g). These were obtained from OPAC, considering a relative humidity of 50% and the composition in table below.

Table 1
The data extracted from OPAC, at a relative humidity of 50%

Aerosol type	Main Components	Number ratio
Desert Dust (depolarizing particles)	Mineral-transported	0.1
	Mineral-nucleation mode (a mixture of quartz and clay minerals)	0.1
	Water soluble (sulfates, nitrates & other water-soluble substances)	0.9
Smoke (non-depolarizing particles)	Water-soluble	0.5
	Soot (absorbing black carbon)	0.5

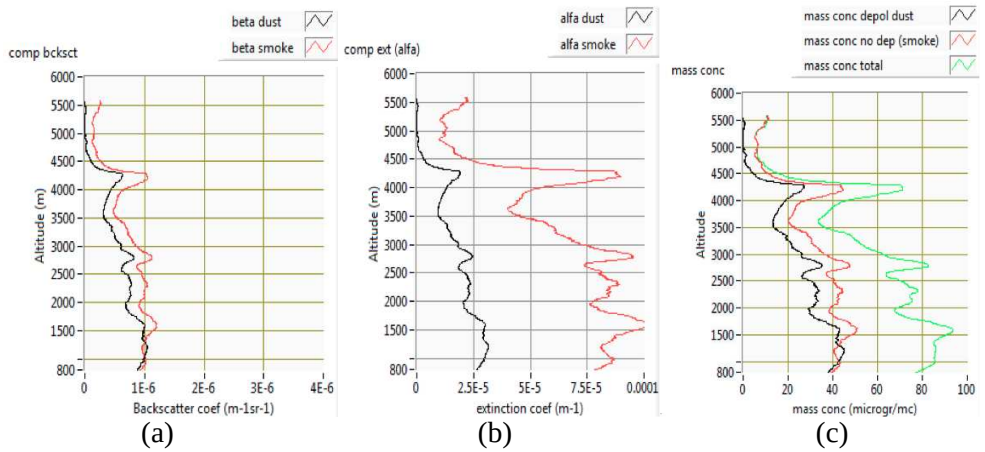

Fig. 2 - Vertical backscatter (a), extinction (b) and mass concentration (c) profiles of the depolarizing (black line) and non depolarizing (red line) particles above Magurele, July 11th, 2012, 23:32 - 00:02 UTC. Total mass concentration is in green.

From the graphs above we see that an almost equal proportion of dust and smoke particles are present in the Planetary Boundary Layer, up to 1300 m altitude. The dust particles found in the first hundred meters above ground are produced mostly by traffic and construction industry nearby the measurement station. Soil dust is similar in composition to the mineral dust, but has an increased content of organic matter, constituted mainly of remains of micro-organisms that participated in degrading plant debris before their own decay.

Smoke (small, highly absorbing particles) is always present near to the ground due to combustion processes, both industrial and housing. Dust and smoke are well mixed within PBL. The proportion depends on the seasonal specific anthropogenic activities and local meteorology.

In the free troposphere, the content of dust / smoke is less influenced by the local sources, and much more by the long-range transport. In the case above, the layers from 1300 m to 4500 m are characterized by a high content of smoke-like particles, which is confirmed by the high Angstrom parameter obtained from sun photometer, Fig. 3a.

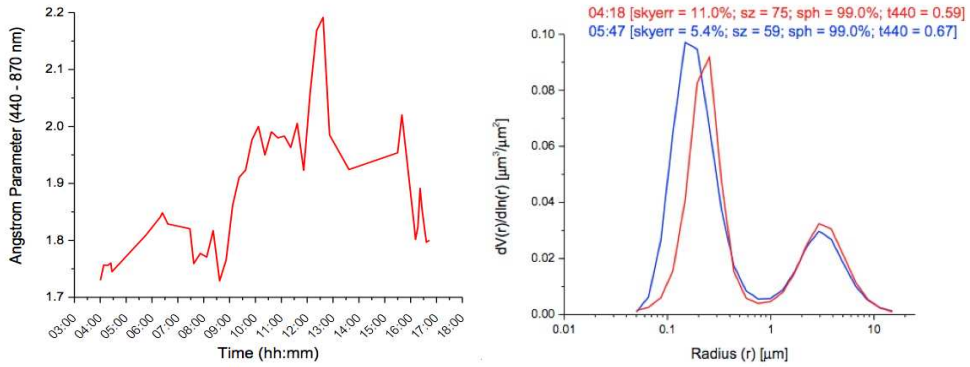

Fig. 3 - (a) Angstrom parameter and (b) Column average size distribution obtained from sunphotometer, in Magurele, July 11th, 2012.

Time series from sunphotometer in Fig. 3a show an important increase of the Angstrom parameter around 9 a.m. UTC that day, which is probably the approximate time of arrival of the contaminated air masses. A mean layer value of 1.8 ± 0.3 was obtained from lidar optical data around midnight. High values of the Angstrom exponent indicating fine particles are consistent with the size distribution obtained by inversion of the multiwavelength sun photometer data, which shows a strong peak of the fine mode, Fig. 3b. Nevertheless, the coarse mode is also represented in the size distribution, corresponding to a low content of dust. Overall, the fine mode is predominating. High values of the AOD from the sun-photometer would be expected to indicate highly absorbing particles, but this parameter was around 0.5 before sunset.

The AOD is an extensive parameter, i.e. depends on the particle type but also on the columnar load. Considering a mass concentration of about 40 $\mu g/m^3$ confined inside the layer, the sensitivity of this parameter to the presence of smoke particles is sufficiently low to not be conclusive.

Confirmation of the aerosols' origin in the mixed layer combined of smoke (predominating) and dust particles are the backward trajectories obtained from HYSPLIT (Fig. 4a) and the MODIS FIRE map (Fig. 4b). Note that air mass trajectories in the free troposphere arriving on July 11th, 2012 at Magurele, originate from South Europe (Fig. 4a), where MODIS detected a high density of forest fires during the last 10 days (indicated with red points) (Fig. 4b). Trajectories come from low altitudes and do not encounter precipitation on the path. As consequence, there is a high chance that they were collecting smoke particles while passing over fires, mixing them with continental polluted aerosols, which are typical for Europe.

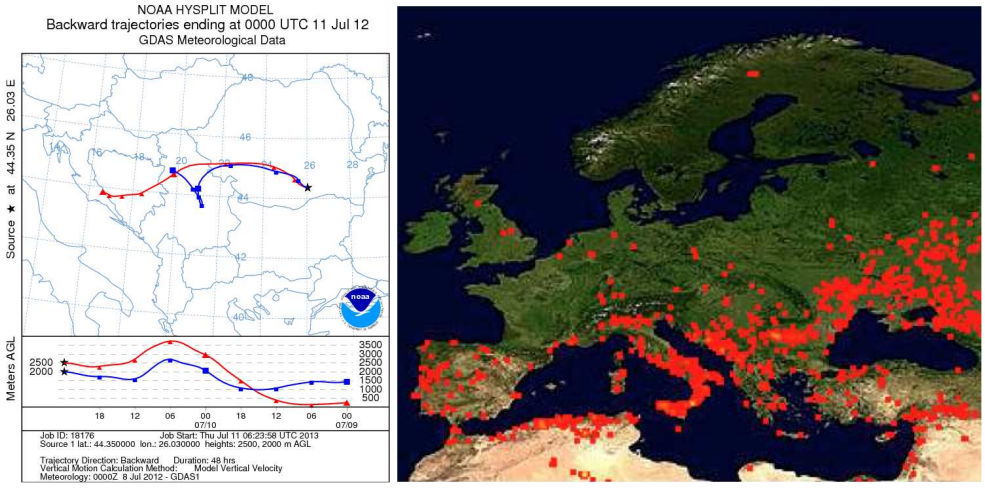

Fig. 4 - Source of aerosol particles: a) HYSPLIT backtrajectories for July 11th, 2012; b) MODIS firemaps, 10 days integration.

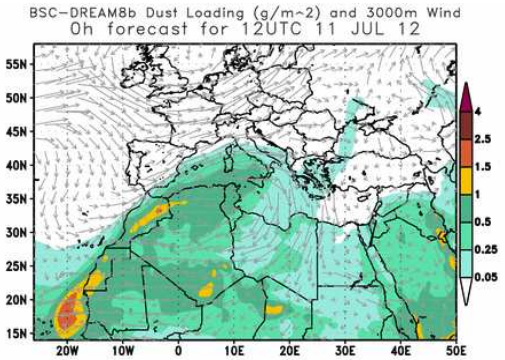

Fig. 5 - Saharan dust loading by DREAM forecast for July 11th, 2012, 23:00 UTC - 00:00 UTC.

The DREAM model does not confirm a significant concentration of Saharan dust over Romania for that day (Fig. 5), but a certain amount of mineral dust was forecasted for South Europe. This may explain the presence of a small content of depolarizing particles in the free troposphere layers above the lidar station, mixed with biomass burning aerosols.

Case 2.Dust event from July 15th, 2012 at Magurele

Sahara is the world's largest source of airborne mineral dust [21]. Its transport over Europe has a clear seasonality, being more frequent from February to June and from late autumn to early winter although dust events can be distributed throughout the year [22]. Romania is frequently affected by Saharan dust episodes. Due to the long path from the source, mineral dust particles are generally mixed with other particles, such as continental pollution and smoke. As consequence, the optical properties of lofted dust layers never match the properties of pure Saharan dust, although mineral particles are hardly reactive and hygroscopic. A typical dust intrusion event is shown in the next graphs for July 15th, 2012.

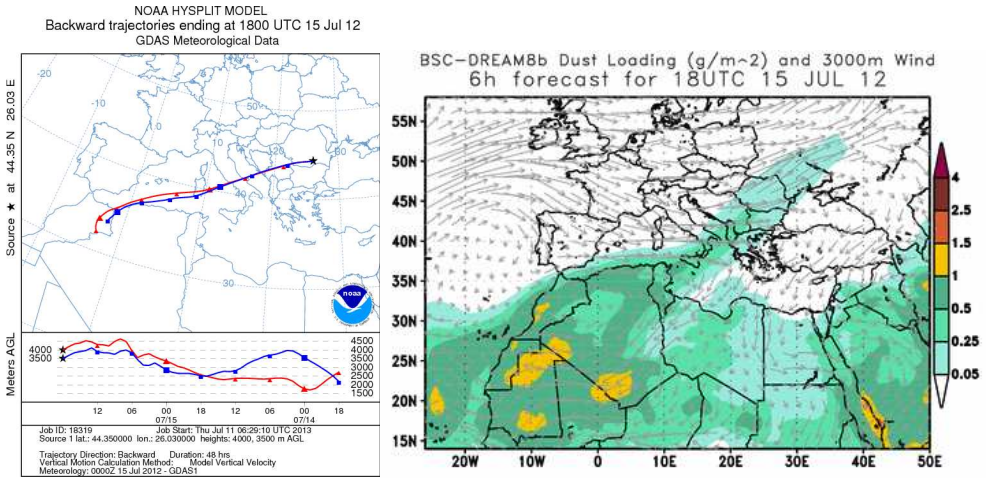

(a) (b)

Fig. 6 - Source of aerosol particles for July 15th, 2012: a) HYSPLIT backward trajectories; b) DREAM Saharan dust loading.

The presence over Romania of near directly transported dust from the Saharan Desert is confirmed firstly by HYSPLIT backward trajectories (Fig. 6a) and secondly by the forecast model DREAM (Fig. 6b). The presence of dust in the atmosphere over Magurele was detected by the multiwavelength lidar system.

The figure 7a and 7b show the range corrected signals at 1064nm, respectively the 532 nm linear volume depolarization. The black lines in figure 7a correspond to the top of the layers. Note that the well-defined layer between 2500 – 5000 m is characterized by a high depolarization, which is consistent to the presence of Saharan mineral dust.

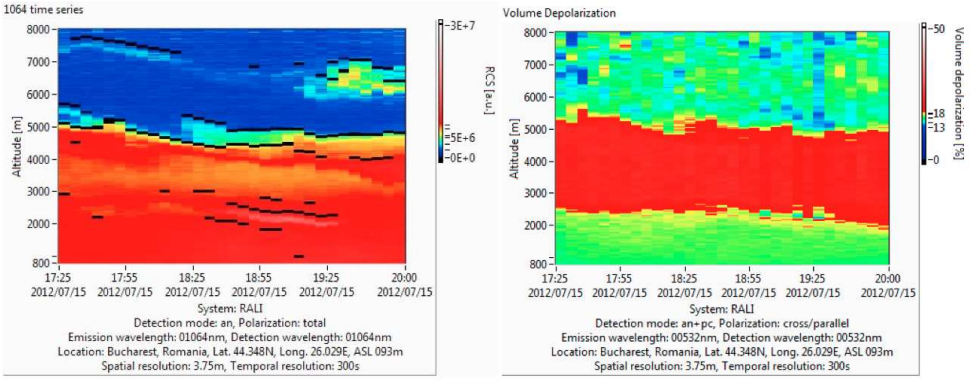

(a) (b)

Fig. 7 - Vertical and temporal distribution of aerosol layers on July 15th, 2012: a) 1064 nm range corrected signal and b) 532 nm linear volume depolarization measured by the lidar.

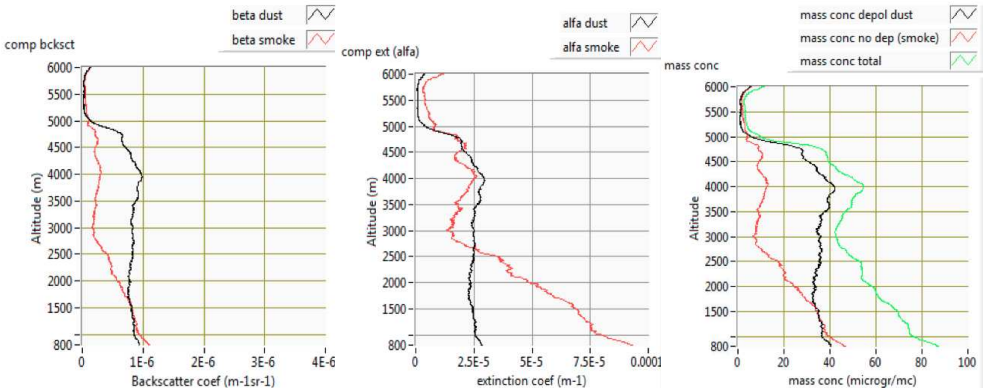

(a) (b) (c)

Fig. 8 - Vertical backscatter (a), extinction profiles (b) and mass concentration (c) of the depolarizing (black line) and non depolarizing (red line) particles above Magurele, July 15th, 2012, 18:00 UTC - 19:00 UTC. Total mass concentration is in green.

Applying the theory introduced in Tesche et al. [8] and described above, we calculated as in the previous case backscatter and extinction coefficient vertical profiles for depolarizing and non-depolarizing particles (Fig. 8a, Fig. 8b), as well as mass concentration profiles (Fig. 8 c).

In this particular case, a quantitative validation of the obtained dust concentration profile was performed through the estimation of total atmospheric column dust loading, by considering an average calculated mass concentration of 35 $\mu g/m^3$ up to a height of 5000 m (Fig. 8c) and zero dust concentration above this height. The obtained value, 0.175 g/m^2, fell within the range forecast by DREAM for Romania, i.e. 0.05-0.25 g/m^2, with the higher values more likely for the south of the country, including Magurele (Fig. 6b).

As in the previous case, the content of dust and smoke within the PBL is almost equal, due to the contribution of local sources and strong mixing. Above 1500 m, the mass concentration of fine (smoke) particles decreases exponentially, while the mass concentration of dust particles increases, up to 5000 m. Note that the dust layer is clearly evidenced in the backscatter profiles (Fig. 8a) but not visible in the extinction profiles (Fig. 8b). This is due to the fact that the backscatter describes the scattering properties of the dominant aerosol, while the extinction is related to the absorbing properties. Mineral dust is a strongly scattering and a poorly absorbing type of aerosol.

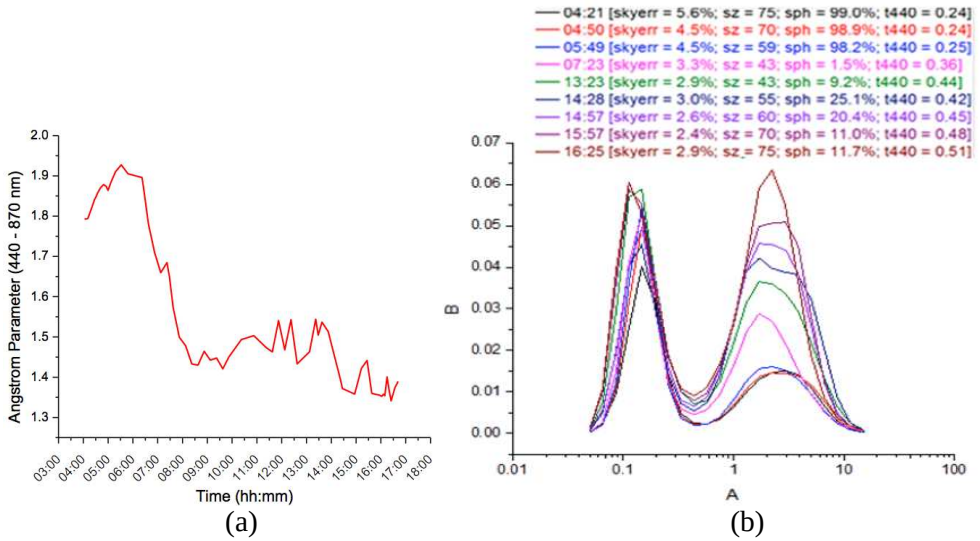

(a) (b)

Fig.9 - Angstrom exponent (a) and columnar average size distribution (b) obtained from sunphotometer in Magurele, July 15th, 2012.

The Angstrom exponent obtained from lidar (not shown) has lower values from 2000 to 3500 m, compared to the PBL (1.7 ± 0.3 below 2000 m, and 0.8 ± 0.2 above).

This is again consistent to the column averaged Angstrom exponent obtained from the sun photometer (Fig. 9a). Note that a sharp decrease of the Angstrom exponent occurs around 08:00 UTC, the probable time of arrival of the long-range transported particles. Due to the daytime operation of the sunphotometer and the nighttime operation of the lidar, the values are not directly comparable, but the decreasing trend of the Angstrom parameter from sun photometer is a good estimator of the agreement between the two instruments.

The Angstrom Exponent (Fig. 9a) and the size distribution (Fig. 9b) for July 15th, 2012, with a strong peak for the coarse mode indicate the presence of large particles. No conclusion can be drawn from the sun photometer AOD, with values around 0.4 at 500 nm. As in the previous case, the columnar load was too low to influence drastically the AOD.

CONCLUSIONS

The method proposed by Tesche, combined with forward simulations (i.e. OPAC) has been used to assess the mass concentration using optical data. Based on complementary information (e.g. preliminary assessment of aerosol source from forecast models and backward trajectories) and optical coefficients (Angstrom exponent, lidar ratio, particle depolarization, AOD), aerosol layers can be investigated as a mixture of depolarizing and non-depolarizing particles. The total mass concentration is computed using mass-extinction efficiencies.

Two different cases (biomass burning and Saharan dust) are presented and the obtained optical parameters were validated by various data sources (DREAM, HYSPLIT, AERONET, MODIS).

Although other cases have to be analyzed before a clear conclusion is drawn, the method seems to be reliable and accurate enough, when necessary assumptions are mad.

Acknowledgements

This work was supported a grant of the STAR–ESA Programme 38/2012-CAPESA and by the strategic grant POSDRU/159/1.5/S/137750, Project "Doctoral and Postdoctoral programs support for increased competitiveness in Exact Sciences research" cofinanced by the European Social Found within the Sectorial Operational Program Human Resources Development 2007 – 2013.

REFERENCES

1. O. Dubovik, B. Holben, T. F. Eck, A. Smirnov, Y. J. Kaufman, M. D. King, D. Tanre, I. Slutsker, J. Atmos. Sci. **59**, 590–608 (2002).
2. J. H. Seinfeld and S. N. Pandis, *Atmospheric Chemistry and Physics, From Air Pollution to Climate Change*, John Wiley & Sons, New York, 1998.
3. D. Muller, U. Wandinger, A. Ansmann. Applied Optics **38** (12), 2346-2357 (1999).
4. D. Muller, U. Wandinger, A. Ansmann, Applied Optics **38** (12), 2358-2368 (1999)
5. J. Wagner, A. Ansmann, U. Wandinger, P. Seifert, A. Schwarz, M. Tesche, A. Chaikovsky, O. Dubovik, Atmos. Meas. Tech. Discuss., **6**, 911–948 (2013).
6. J. L. Hand and W. C. Malm, J. Geophys. Res. **112**, D16203 (2007).
7. C. Bockmann, D. Muller, L. Osterloh, P. Pornsawad, A. Papayannis, Geoscience and Remote Sensing Symposium, IEEE International 2, 422-425, (2008).
8. M. Tesche, A. Ansmann, D. Müller, D. Althausen, R. Engelmann, V. Freudenthaler, S. Groß, J. Geophys. Res. **114**, D13202 (2009).
9. A. Ansmann, P. Seifert, M. Tesche, U Wandinger.. Atmos. Chem. Phys. **12**, 9399–9415 (2012).
10. M. Hess, P. Koepke, I. Schult, Bull. Am. Met. Soc. **79**, 831–844 (1998).
11. G. Pappalardo, Feature article in EARSeL Newsletter **82**, 13-18 (2010).
12. C. Radu, L. Belegante, C. Talianu, D. Nicolae, J.Optoelectron. Adv.Mater. **12**(1), 165-168 (2010).
13. L. Belegante, C. Talianu, A.V. Nemuc, D. Nicolae. Rom. Journ. Phys. **56** (3-4), 484-494 (2011).
14. J. Biele, G. Beyerle, G. Baumgarten, Opt. Expr. **7**, 427–435 (2000).
15. V. Freudenthaler, M. Esselborn, M. Wiegner, B. Heese, M. Tesche, A. Ansmann, D. Müller, A. Althausen, M. Wirth, A. Fix, G. Ehret, P. Knippertz, C. Tolenado, J. Gasteiger, M. Garhammer, M. Seefeldner, Tellus **B61**, 165– 179 (2009).
16. M. Tesche, A. Ansmann, D. Müller, D. Althausen, I. Mattis, Tellus **B61**, 144 – 164 (2008).
17. A. Nemuc, J. Vasilescu, C. Talianu, L. Belegante, D. Nicolae, Atmos. Meas. Tech. Discuss. **6**, 5923-5957 (2013).
18. S. Nickovic, A. Papadopoulos, O. Kakaliagou, G. Kallos, J. Geophys. Res. **106**, 18113–18129 (2001).
19. S. Ilavajhala, M. M. Wong, C.O. Justice, IEEE Transactions on Geoscience and Remote Sensing. **47**(1), 72-79 (2009).
20. Y. J. Kaufmann, D. Tanre, O. Boucher, Nature **419**, 215-223 (2002).
21. G.A. D'Almeida, *Desert aerosol characteristics and effects on climate*. In: M. Leinen, M. Sarnthein (Eds.), Palaeoclimatology and Palaeometeorology:

Modern and Past Patterns of Global Atmospheric Transport. NATO ASI Series **C282**, 311-338 (1987).

22. M. Escudero, S. Castillo, X. Querol, A. Avila, M. Alarcon, M.M. Viana, A. Alastuey, E. Cuevas, S. Rodriguez, J. Geophys. Res. **110** (D18S08) 1-15 (2005).